

## Synthetic baseline navigation using phase-coherent acoustic communication signals

Eric Gallimore, Mark Anderson, Lee Freitag, and Eric Terrill

Citation: *The Journal of the Acoustical Society of America* **146**, 4831 (2019); doi: 10.1121/1.5137902

View online: <https://doi.org/10.1121/1.5137902>

View Table of Contents: <https://asa.scitation.org/toc/jas/146/6>

Published by the [Acoustical Society of America](#)

---

### ARTICLES YOU MAY BE INTERESTED IN

[Bathymetry-aided underwater acoustic localization using a single passive receiver](#)

*The Journal of the Acoustical Society of America* **146**, 4774 (2019); <https://doi.org/10.1121/1.5138605>

[Bayesian coherent and incoherent matched-field localization and detection in the ocean](#)

*The Journal of the Acoustical Society of America* **146**, 4812 (2019); <https://doi.org/10.1121/1.5138134>

[Introduction to the Special Issue on Acoustic Source Localization](#)

*The Journal of the Acoustical Society of America* **146**, 4647 (2019); <https://doi.org/10.1121/1.5140997>

[Demonstration of spiral wave front sonar for active localization](#)

*The Journal of the Acoustical Society of America* **146**, 4821 (2019); <https://doi.org/10.1121/1.5138132>

[Automated localization of whales in coastal fjords](#)

*The Journal of the Acoustical Society of America* **146**, 4672 (2019); <https://doi.org/10.1121/1.5138125>

[Convolutional neural network for single-sensor acoustic localization of a transiting broadband source in very shallow water](#)

*The Journal of the Acoustical Society of America* **146**, 4687 (2019); <https://doi.org/10.1121/1.5138594>

---

SUBMIT TODAY!

**JASA**  
THE JOURNAL OF THE  
ACOUSTICAL SOCIETY OF AMERICA

**Special Issue: Theory and  
Applications of Acoustofluidics**

# Synthetic baseline navigation using phase-coherent acoustic communication signals

Eric Gallimore,<sup>1,a)</sup> Mark Anderson,<sup>2</sup> Lee Freitag,<sup>3</sup> and Eric Terrill<sup>1</sup>

<sup>1</sup>*Scripps Institution of Oceanography, University of California, San Diego, 9500 Gilman Drive, La Jolla, California 92093, USA*

<sup>2</sup>*Department of Mechanical and Aerospace Engineering, University of California, San Diego, 9500 Gilman Drive, La Jolla, California 92093, USA*

<sup>3</sup>*Department of Applied Ocean Physics and Engineering, Woods Hole Oceanographic Institution, 266 Woods Hole Road, Woods Hole, Massachusetts 02543, USA*

(Received 12 September 2018; revised 9 January 2019; accepted 16 January 2019; published online 31 December 2019)

The development of a synthetic baseline navigation technique that self-localizes an autonomous underwater vehicle (AUV) using intermittent acoustic communications signals received by a single transducer is described, along with field results from in-ocean tests. The method uses the phase measurement at the output of a second-order phase-locked loop to create fine-scale pseudorange estimates in addition to, or in the absence of, a one-way travel time measurement based on the arrival time of the acoustic data packet. These range measurements are incorporated by an adaptive particle filter. This technique allows the vehicle navigation system to take advantage of multiple phase-derived range measurements made over the duration of a communication packet. These measurements, when incorporated with an appropriate filter and vehicle kinematic model, improve vehicle navigation at no additional cost in navigation-specific acoustic transmissions. This approach was demonstrated and evaluated with data collected at-sea using a REMUS 100 AUV (Hydroid, Inc., Pocasset, MA). © 2019 Acoustical Society of America. <https://doi.org/10.1121/1.5137902>

[KTW]

Pages: 4831–4841

## I. INTRODUCTION

Autonomous underwater vehicles (AUVs) have traditionally relied on acoustic navigation techniques such as long-baseline (LBL) or ultra-short-baseline (USBL) systems, which require measuring two-way acoustic travel times between multiple transmit or receive elements to form a navigation solution (Austin, 1994; Fulton, 2000). These techniques generally form least-squares maximum likelihood estimates of position using a well-constrained set of time-delay-of-arrival measurements.

The use and development of accurate and synchronized clocks has enabled one-way travel time (OWTT) measurements that are suitable for navigation (e.g., Eustice *et al.*, 2006, 2007). Various systems have been developed that employ a single estimate of the OWTT of an acoustic communications packet rather than a signal dedicated to navigation (Eustice *et al.*, 2006, 2007; Singh *et al.*, 2006; Stojanovic *et al.*, 2002). These systems offer several advantages over traditional LBL and USBL navigation: they reduce the number of acoustic transmissions required, are scalable to any number of receivers, and eliminate one path delay to reduce latency. Navigation solutions using OWTT may use one or several transmitters, depending on the implementation and its desired accuracy and spatial coverage.

Synthetic baseline navigation computes a localization solution by leveraging the motion of either the AUV or another platform to provide multiple range measurements over time. This has been demonstrated using two-way travel time to transponders (Hartsfield, 2005; Larsen, 2000) and

with USBL-style direction-of-arrival measurements (Watanabe *et al.*, 2009a, 2009b; Watanabe *et al.*, 2012). A primary objective of these methods is to reduce the number of acoustic emitters, ideally to one, or improve the quality of the navigation solution for a given number of transponders or navigation beacons. Similar techniques have been used to localize moving sources using fixed receive arrays that exploit acoustic channel structure (Yang, 2015). Generally, the navigation solution is computed using linear estimators (least squares or Kalman filters) that incorporate range measurements, a model of vehicle kinematics, and other sensor inputs available on a platform. Recently, particle filters have been used to improve performance of traditional USBL navigation systems coupled with other navigation aids such as a Doppler velocity log (DVL; Rigby *et al.*, 2006).

The work presented here builds upon the navigation methods reviewed above. Importantly, it relies only on phase tracking information, which is often already available from Doppler estimators in acoustic communications receivers. The specific approach presented here takes advantage of the phase-locked loop (PLL) incorporated in a decision-feedback equalizer in a single-carrier communications receiver but could be adapted to other modulation methods that use high-resolution Doppler estimators.

This approach enables localization using acoustic communication signals when OWTT is not available, and it is therefore useful when synchronized transmit and receive clocks are not available. When OWTT measurements are available, this technique reduces the uncertainty of the position estimate, which enables localization using fewer acoustic transmissions.

<sup>a)</sup>Electronic mail: egallimore@whoi.edu

## II. IMPLEMENTATION

The navigation system, described in detail in this section, uses an adaptive particle filter to estimate vehicle position. The process model is based on the vehicle kinematics and incorporates a seven-variable state vector along with control inputs. High-resolution pseudorange measurements are computed using the phase tracking output of the acoustic receiver while communication packets are being received. The measurement model incorporates these pseudorange measurements, along with an initial starting range derived from the OWTT of the communication packet, if it is available, velocity information from the vehicle's DVL, and heading information from the vehicle attitude and heading reference system (AHRS). Localization of the vehicle is achieved using a hybrid particle filter where position is tracked by a particle filter, and other state variables are tracked using an unscented Kalman filter (UKF).

### A. Kinematic process model

The vehicle is localized using a two-dimensional constant turn rate and velocity kinematic model that also incorporates horizontal water current. A complete description of the dynamics of an underwater vehicle involves 18 state variables, and current (fluid velocity) requires at least 3 more.<sup>1</sup> For both conceptual and computational simplicity, the model tracks only a subset of the state, which is sufficient to track the vehicle.

Depth is not explicitly tracked in this model, although it is indirectly incorporated in some measurement functions of the tracking filter. This assumption is reasonable as the depth of the vehicle can be measured with high precision and accuracy using a pressure transducer. Furthermore, the vehicle sway velocity is incorporated in the current velocity terms. As the vehicle uses only one thruster, which propels the vehicle forward or backward and cannot directly induce transverse motion, any sway over ground is due primarily to ocean currents.

The vehicle surge velocity (forward, through water), yaw, and yaw rate are composed in the body-fixed frame, while the current velocity and vehicle position are in local north-east-down (NED) coordinates. The corresponding state vector is

$$\mathbf{x} = \begin{bmatrix} \text{position, north} \\ \text{position, east} \\ \text{current velocity, north} \\ \text{current velocity, east} \\ \text{vehicle surge velocity} \\ \text{vehicle yaw (heading angle)} \\ \text{vehicle yaw rate} \end{bmatrix} = \begin{bmatrix} x \\ y \\ u_C \\ v_C \\ u \\ \psi \\ r \end{bmatrix}. \quad (1)$$

The vehicle control inputs include speed and steering control, corresponding to the rotational rate of the propeller and the angle of the rudder

$$\mathbf{u} = \begin{bmatrix} \text{propeller speed} \\ \text{rudder angle} \end{bmatrix} = \begin{bmatrix} n \\ \delta_r \end{bmatrix}. \quad (2)$$

With these controls, the speed model is

$$u = b_u(n), \quad (3)$$

where  $b_u$  is an empirically determined function mapping propeller rotation rate to vehicle speed through water. The steering model is

$$r = b_\delta(\delta_r), \quad (4)$$

where  $b_\delta$  is an empirically determined function mapping rudder angle to vehicle yaw rate. Both of these empirical functions can be determined by performing a polynomial fit to experimental data collected on the vehicle over a range of speed and steering inputs.

The horizontal position is calculated using the kinematic differential equations

$$\dot{x} = u_C + u \cos \psi, \quad (5)$$

$$\dot{y} = v_C + u \sin \psi, \quad (6)$$

and the yaw and yaw rate are related as

$$\dot{\psi} = r. \quad (7)$$

### B. Pseudorange measurement via phase tracking

The navigation technique exploits the phase tracking information required to properly demodulate and equalize a phase-shift keyed (PSK) communications packet, which is made available from a PLL. The approach is independent of the type of signal constellation, and it may be binary phase-shift keying (BPSK), quadrature phase-shift keying (QPSK), or higher order. This output of the PLL is a phase time series that can be used to generate hundreds of estimates of the range between the transmitter and receiver for each packet, depending on the length of the packet and its bandwidth.

Typical PSK packets begin with an acquisition probe [such as a frequency-modulated (FM) sweep], followed by a PSK-modulated sequence that includes an equalizer training sequence and coded data.

The implementation described here is based on the processing done by a Woods Hole Oceanographic Institution (WHOI, Woods Hole, MA) Micromodem-2 acoustic modem. In this system, the acquisition probe is detected using a matched filter, and the modem determines and reports a time-of-arrival (TOA) that corresponds to this detection. If clocks at the transmitter and receiver are synchronized, this process alone can be used to determine OWTT for navigation purposes (Singh *et al.*, 2006). The Micromodem-2 provides time-of-arrival measurements with one microsecond precision and to the accuracy governed by the bandwidth and acoustic propagation channel. The modem clock can be synchronized with a reference, such as a pulse-per-second signal from a global positioning system (GPS) at the start of a mission, or a stable atomic clock in the vehicle (Gallimore *et al.*, 2010).

The initial range estimate for each packet is made using the TOA measurement for the acquisition probe. Using the known time of transmission, this forms a single OWTT measurement, assuming a direct acoustic path. This implementation uses the local speed of sound [as measured by the AUV

via a conductive, temperature, and depth (CTD) sensor] to determine a corresponding geometric range, but this can be improved by the use of ray tracing to compute the average sound speed over the path taken by the signal from its source.

The QPSK sequence is processed using an adaptive equalizer that incorporates a least-mean-squares (LMS) adaptive filter and a second-order PLL for carrier phase tracking. The equalizer estimates the channel impulse response and applies a corresponding filter to the incoming samples such that the channel effects are mitigated. The PLL phase gradient is calculated by measuring the phase difference between the received QPSK symbol, as demodulated using the PLL-adjusted carrier, and a known training symbol. Each packet incorporates a direct-current-balanced training sequence chosen to enable this carrier recovery. The PLL is tuned such that most of the motion-induced Doppler shift is tracked by the PLL, and not by the group delay of the LMS filter, using parameters from Johnson *et al.* (1997). This process is illustrated in Fig. 1. A more detailed discussion of the adaptive equalizer can be found in Stojanovic *et al.* (1994).

The PLL-tracked phase is then low-pass filtered and delay corrected. The phase measurement controls a resampling filter that applies a corresponding group delay (positive or negative) to the incoming samples such that time dilation or contraction is removed. The group delay ( $T$ ) associated with this phase shift is given as

$$T = -\frac{\phi}{2\pi f_c}, \quad (8)$$

where  $\phi$  is the phase shift and  $f_c$  is the carrier frequency.

In this method, the calculated group delay is tracked throughout the received packet and is used indirectly to generate pseudorange measurements for each received symbol at a decimated rate that is chosen to match the cutoff frequency of the low-pass phase filter.

It should be noted that the measurements are only valid if the equalizer has converged and is operating with reliable feedback. If not, the phase gradient measurement may be invalid, and this error will propagate into the group delay estimate. Typically, the equalizer converges during training, where perfect feedback is available, and then continues to operate

reliably after changing to decision-directed mode. To test that the measurements are valid, the equalizer mean-squared error (MSE) is low-pass filtered to provide a reliable low-noise estimate, and when the MSE for a symbol is low (less than 1, corresponding to positive output signal-to-noise ratio, SNR), the equalizer is in a converged state. In this state, the algorithm considers the group delay estimate for that symbol to be valid.

The local speed of sound is used to convert each filtered and gated group delay measurement to a difference in range between subsequent received symbols. This process yields a series of range measurements between the source and receiver over the duration of the received packet, which are then used in the Bayesian tracking filter to localize the AUV.

### C. Measurement models

The measurement models incorporate the phase-derived pseudorange measurements, OWTT measurements, and data from the vehicle's DVL and AHRS. An appropriate model is selected to incorporate only the measurements that are available in each time step.

The pseudoranges to each transmitting source are calculated using the phase tracking method described above. The range relation is given as

$$\rho = \sqrt{(x_{\text{source}} - x)^2 + (y_{\text{source}} - y)^2 + (z_{\text{source}} - z)^2}, \quad (9)$$

where  $\rho$  is the range, and  $x$ ,  $y$ , and  $z$  are distances in Cartesian space. The vertical components ( $z$ ) are not modeled but are used directly by the measurement functions.

The DVL reports the bottom tracking velocity in the body frame: surge velocity  $u_{\text{DVL}}$  and sway velocity  $v_{\text{DVL}}$ . These are related to state as

$$u_{\text{DVL}} = u + u_C \cos \psi + v_C \sin \psi, \quad (10)$$

$$v_{\text{DVL}} = u_C \sin \psi + v_C \cos \psi. \quad (11)$$

The vehicle AHRS measures yaw rate and heading angle (adjusted to true north) as

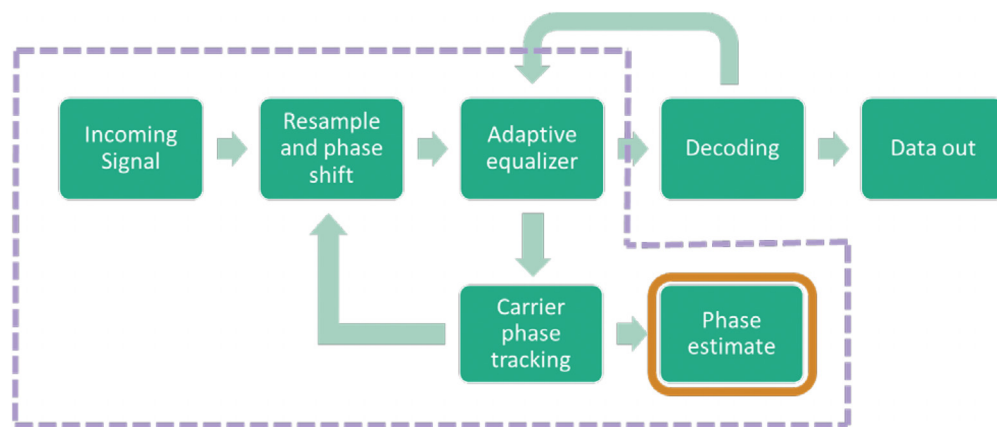


FIG. 1. (Color online) Block diagram showing basic processes involved in receiving phase-shift keyed (PSK) acoustic communication signals. The portion of this process that is used for navigation in this work is enclosed within the dashed line.

TABLE I. Summary of measurements and instruments used for navigation with their update rates, standard deviation, and availability.

Measurement	Instrument	Typical measurement rate	Typical standard deviation	Availability
Range from OWTT	Acoustic communication system with synchronized clocks	<0.1 Hz	0.01–10 m (depending on time synchronization and error sources described in text)	Intermittently, once each time a packet is received (if transmit and receive time are synchronized)
Difference in range from phase tracking information	Acoustic communication system	Up to phase-shift keyed (PSK) symbol rate	0.00012 m	During packet reception for approximately 3.5 s
Velocity over ground	DVL (1200 kHz RDI Workhorse ADCP, Teledyne RD Instruments, Poway, CA)	0.5–2 Hz	0.3 cm/s (Teledyne RD Instruments, 2016)	When vehicle is <25 m above seafloor
Yaw (heading) and heading rate	AHRS (Kearfott INS, Kearfott Corporation, Woodland Park, NJ) or magnetic compass	9–10 Hz	0.1 (INS)–3 deg (magnetic compass)	Continuous

$$r_{\text{gyro}} = r, \quad (12)$$

$$\psi_{\text{compass}} = \psi. \quad (13)$$

We assume that measurement noise is normally distributed for each of these instruments, and each of them reports data at different rates, as summarized in Table I.

#### D. Localization with hybrid particle filter

Tracking and localization of vehicles is commonly performed using Kalman filters to estimate position and velocity. When the system being modeled includes nonlinear states or measurements, extensions of the Kalman filter are often employed, such as the extended Kalman filter (EKF) and the UKF (Julier and Uhlmann, 1997). The UKF improves upon the EKF for many systems, and details relating to its performance and implementation are widely discussed in the literature; see, e.g., Gustafsson (2012), Julier and Uhlmann (2004), Simon (2006), and Wan and Merwe (2000).

Despite its advantages over the EKF, the UKF may still perform poorly when applied to some nonlinear systems. In practice, the pseudorange measurement data prove unsuitable for a linear or linearized filter because the corresponding measurement equation (8) is nonlinear, and the associated probability densities can be multimodal and non-Gaussian in Cartesian space.

To avoid some of the problems associated with using a linear filter with a nonlinear system, a particle filter is used to form vehicle location estimates. The particle filter does not assume that the system is linear, Gaussian, or unimodal. Several excellent overviews of particle filters exist; see, e.g., Cappe *et al.* (2007), Gustafsson (2010), Ristic *et al.* (2004), and the implementation used in this system is described below.

However, tracking all the state variables in a particle filter would be computationally prohibitive in an embedded system. To address this, the implementation partitions the state into linear and nonlinear components, which are tracked with an UKF and a sequential-importance-sampling (SIS) particle filter, respectively. The particle filter acts as an integration filter that incorporates the estimate from an UKF, as illustrated in Fig. 2.

In this hybrid filter, the model is simplified such that the particle filter only tracks the following state:

$$\mathbf{x}^p = \begin{bmatrix} \text{position, north} \\ \text{position, east} \end{bmatrix} = \begin{bmatrix} x \\ y \end{bmatrix}. \quad (14)$$

A separate UKF uses DVL, AHRS, and steering data to estimate a state vector,

$$\mathbf{x}^k = \begin{bmatrix} \text{vehicle velocity over ground} \\ \text{vehicle heading over ground} \end{bmatrix} = \begin{bmatrix} v_g \\ \psi_g \end{bmatrix}. \quad (15)$$

The velocity and heading over ground incorporate the effects of both currents and AUV body motion.

The Kalman state estimate is used as a control input to the particle filter in the prediction step as

$$\mathbf{x}_{t+1}^p = f(\mathbf{x}_t^p, \mathbf{x}_t^k, \nu_t), \quad (16)$$

where  $\nu$  is process noise, and  $f$  is a function that predicts the state variables as

$$x_{t+1} = x_t + (v_{g,t} + \nu_{v,t}) \cos \psi_{g,t+1}^p dt, \quad (17)$$

$$y_{t+1} = y_t + (v_{g,t} + \nu_{v,t}) \sin \psi_{g,t+1}^p dt. \quad (18)$$

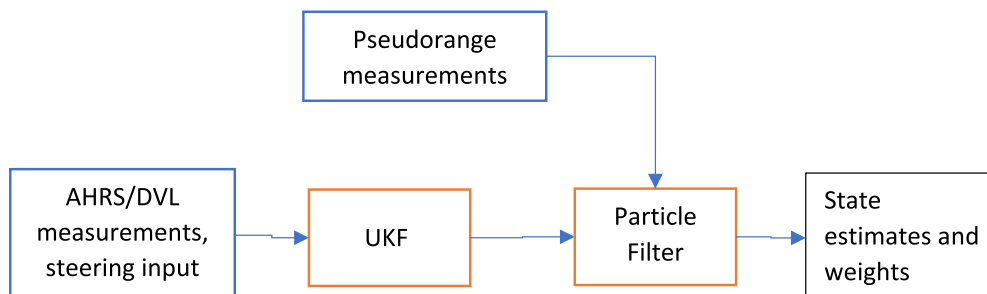


FIG. 2. (Color online) Block diagram showing data flow in the integrating navigation filter using an UKF and a particle filter.

## E. Particle filter measurement update

The measurement update operates in one of two modes. If a OWTT measurement corresponding to a total range is available, the filter adjusts the particle weights using the pseudorange data via the measurement equation (8) and the expressions

$$f_X(x) = \mathcal{N}(\rho_{i,\text{predicted}}, R_\rho), \quad (19)$$

$$w_i = f_X(x), \quad x = \rho_{\text{measurement}}, \quad (20)$$

where  $f_X(x)$  is the probability density function of a normally distributed random variable with mean  $\rho_{\text{predicted}}$  (from the measurement function) and variance  $R$ .  $w_i$  is the particle weight, found by evaluating  $f_X(x)$  at the measurement value.

When using the phase-derived time difference of arrival data, the filter operates instead with the difference in range given by taking the group delay  $T_i$ , from Eq. (8), and multiplying by the speed of sound ( $c$ ) measured by the AUV

$$d\rho_{\text{measurement}} = T_i c. \quad (21)$$

The prior is formed using the control vector output from the UKF to update the nonlinear state vector, as described in Eqs. (17) and (18), and taking the discrete difference of the state across time steps

$$d\rho_{i,\text{predicted}} = \sqrt{(x_{t+1} - x_t)^2 + (y_{t+1} - y_t)^2 + (z_{t+1} - z_t)^2}. \quad (22)$$

Note that  $z$  is not tracked by the filter, but measurements of depth are used directly.

The filter adjusts particle weights in this mode as described above for the OWTT case, but with

$$f_{d\rho}(x) = \mathcal{N}(d\rho_{i,\text{predicted}}, R_{d\rho}), \quad (23)$$

$$w_i = f_{d\rho}(x), \quad x = d\rho_{\text{measurement}}. \quad (24)$$

The particles are roughened (the process is also called jittering or diffusing) by adding additional independent Gaussian noise to prevent sample degeneracy and reduce the effects of dependent noise processes in the sampling system.

In both cases, particle weights are normalized after calculation such that

$$\sum_i w_i = 1. \quad (25)$$

The particles are resampled after each update if the number of effective particles drops too low (below  $N/2$ , where  $N$  is the number of particles), using a common approximation as described in [Gustafsson \(2010\)](#),

$$\hat{N}_{\text{eff}} = \frac{1}{\sum_i w_i^2}, \quad (26)$$

where  $w_i$  is the weight of each particle. Particle resampling is done with a systematic resampler ([Hol et al., 2006](#)).

## F. Position state estimates

Position state estimates are generated by calculating the weighted mean of the particle state vectors

$$\hat{\mathbf{x}}_t^p = \begin{bmatrix} \hat{x}_t \\ \hat{y}_t \end{bmatrix} = \sum_i w_i \begin{bmatrix} x_{i,t} \\ y_{i,t} \end{bmatrix}. \quad (27)$$

Notably, this estimate may not characterize a multimodal distribution in a useful way, so a weighted covariance variance of the state particles is computed to help quantify the validity of the estimate,

$$\mathbf{Q}^p = \frac{1}{1 - \sum_{i=1}^N w_i^2} \sum_{i=1}^N w_i (\mathbf{x}_t^p - \hat{\mathbf{x}}_t^p) (\mathbf{x}_t^p - \hat{\mathbf{x}}_t^p)^T. \quad (28)$$

These position estimates and covariances form the output of the localization system.

## III. SIMULATION

To validate the basic functionality of the localization technique, the filter algorithms were run using simulated vehicle movements across a range of realistic values. This demonstrated that the particle filter could successfully incorporate both OWTT measurements, as well as pseudorange measurements, using the algorithm described in Sec. II. An illustration of the output of the particle filter and estimator from a single acoustic packet simulation is shown in Fig. 3.

## IV. EXPERIMENT AND RESULTS

To evaluate performance of this navigation system under real-world conditions, a REMUS 100 AUV (Hydroid, Inc., Pocasset, MA) was operated in ocean waters adjacent to the Scripps Pier in La Jolla, CA. The vehicle was programmed to swim a north-south and east-west survey pattern (Fig. 4) in constant-altitude mode at a speed of 1.5 m/s for approximately 750 m in each direction. This mission geometry is typical for seabed survey applications using the REMUS 100, and it offered a variety of ranges and aspects between the transmitter and the vehicle.

An acoustic communication gateway buoy (a device that incorporates a subsurface acoustic transducer, an acoustic modem, and a radio link for surface communication) was deployed from the end of a pier, approximately 100 m to the east of the operating area. It transmitted rate 1 Micromodem packets with a 25 kHz carrier, 5 kHz bandwidth, and duration of about 4 s. Packets of this length and type are commonly used for AUV telemetry.

Packets were transmitted at varying intervals throughout the trial with a maximum frequency of four packets per minute. Although more frequent packet transmission could improve the navigation performance, since more phase measurements would be available, the maximum packet frequency was chosen such that there was enough time between transmissions to allow the vehicle's standard LBL navigation and acoustic communication systems to operate during the experiment.

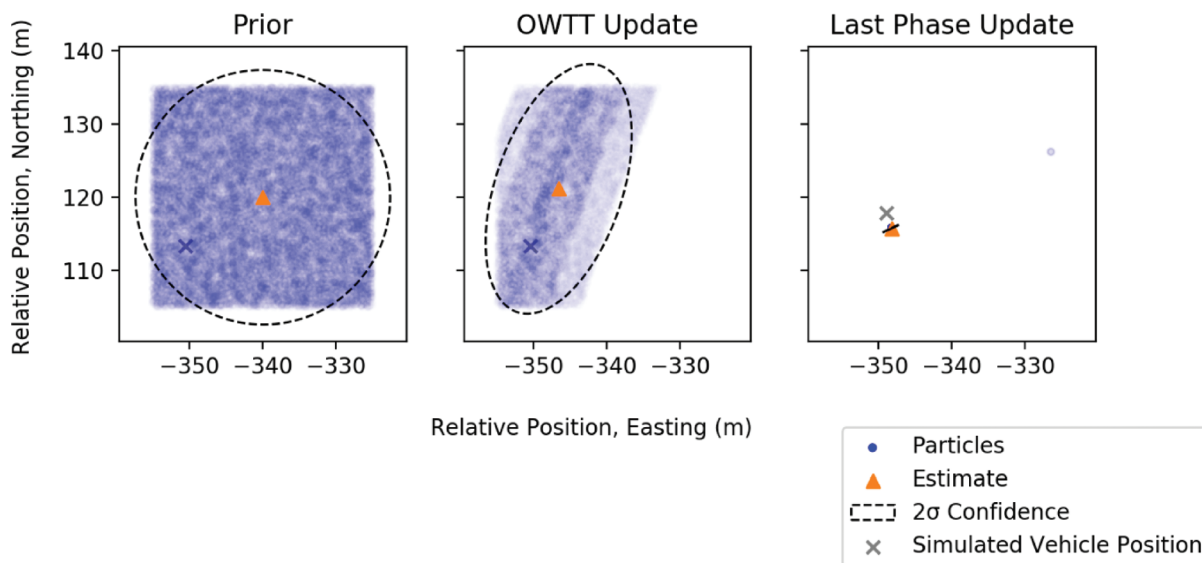


FIG. 3. Plot of particle distributions and navigation filter estimates operating over a single simulated acoustic communications packet of approximately 5 s duration while the simulated vehicle travels at an average of 1.5 m/s. Positions are relative to the simulated transmitter. Each particle (blue dot) is partially transparent with its opacity determined by the weight of the particle. Therefore, darker regions correspond to higher-probability regions. Two-sigma covariance ellipses are drawn with dashed lines. (The covariance ellipse in the right subplot is small and overlaps with the estimate marker.) The weighted estimate, as described in Eq. (27), is plotted as a triangle (orange). The first subplot (“prior”) shows an initial particle distribution, which was deliberately chosen such that it was offset from the simulated position of the vehicle (marked with a cross). The center subplot shows the distribution and estimate associated with the OWTT measurement update, and the corresponding reduction in uncertainty is noticeable. The right plot labeled, “last phase update,” shows the output of the filter after incorporating hundreds of pseudorange measurements. Most of the particles are clustered near the estimated position (and the estimate marker covers most of the dots). Of interest, this example shows an additional cluster of particles near  $-335$  m easting and  $125$  m northing, which represent another less probable position region that remains tracked by the particle filter, illustrating an advantage of this nonlinear filtering technique.

### A. Vehicle hardware

The REMUS vehicle was equipped with a custom passband acoustic recording system that captured data from a single HTI-96 hydrophone (High Tech, Inc., Long Beach, MS) mounted at

the front of the vehicle (Fig. 5). The vehicle is approximately 1.5 m long, and the minimum turning radius is about 5 m.

The hydrophone signal was amplified and filtered by analog circuitry prior to being simultaneously processed by a

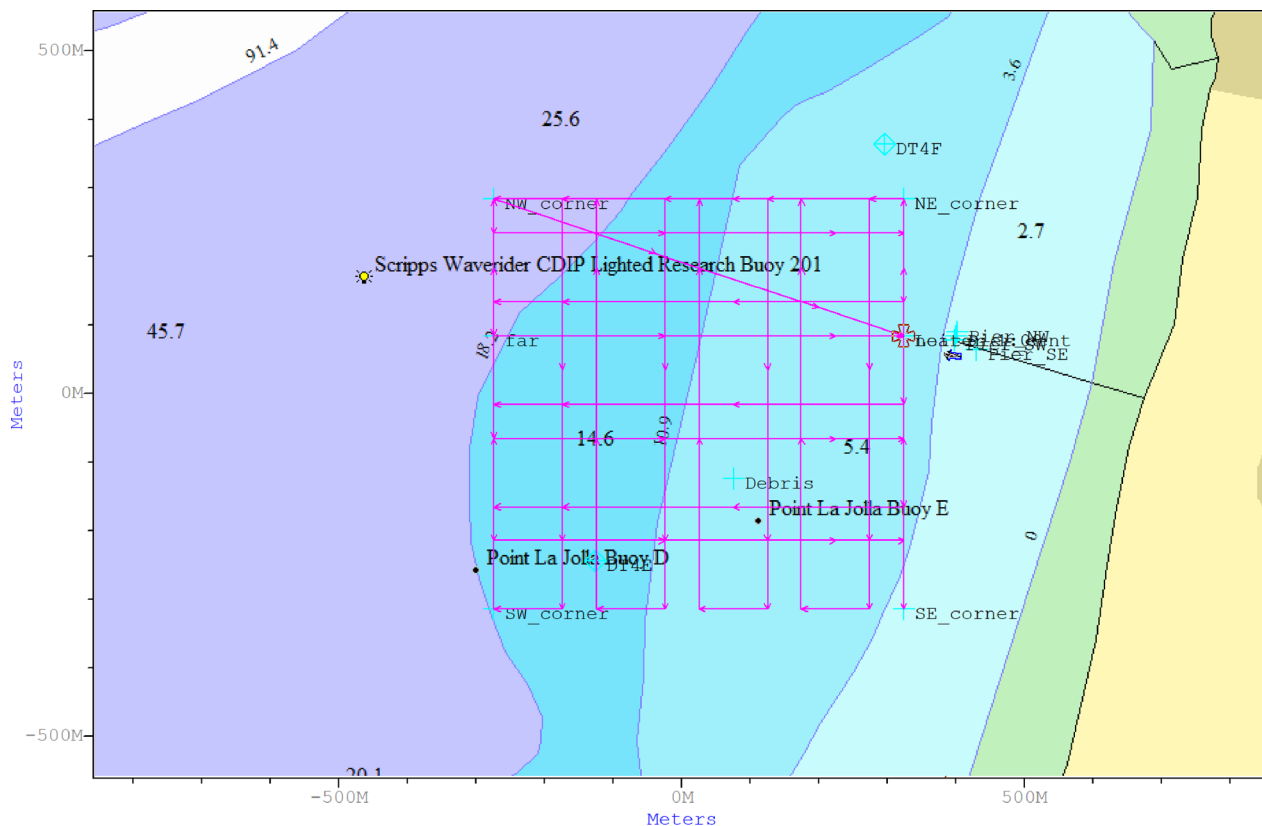


FIG. 4. (Color online) REMUS mission plan. Lines with arrows (magenta) indicate the planned vehicle track. Bathymetry is notated by background shading.

Micromodem-2, which provided GPS-synchronized timestamps for the packet TOA (Gallimore *et al.*, 2012), and sampled by a 96 kHz passband recorder, as illustrated in Fig. 6.

To allow evaluation of the mode in which OWTT is used, a chip-scale atomic clock (CSAC) manufactured by Microsemi Corporation (Aliso Viejo, CA) was incorporated using custom interface hardware. For this experiment, the CSAC was used only as a real-time clock to control drift in the TOA measurements, and not to derive a phase-locked analog-to-digital converter clock.

The acoustic recordings, vehicle AHRS, vehicle DVL, timing information, and additional diagnostic data were logged using a software stack built upon the Robot Operating System (ROS; (Quigley *et al.*, 2009).

These data were processed offline using the navigation filters described above, and the results were compared with the vehicle internal navigation track. The vehicle's internal navigation solution was formed by proprietary algorithms incorporating sensor data (from the vehicle AHRS, GPS when surfaced, and DVL) as well as intermittent LBL transponder fixes.

## B. Results using adaptive filter incorporating OWTT

During the aforementioned mission, the filter was found to capably incorporate data from both the OWTT measurements and phase measurements. The progression of measurement updates as two packets are received is shown in Figs. 7 and 8. In this example, 10 000 particles are generated and randomly distributed uniformly over a 900 m<sup>2</sup> area. The vehicle's actual position falls within this area (but not at its center). In most applications, the initial particle distribution should be chosen such that it adequately samples the possible locations of the vehicle. These experimental results suggest that an initial particle density between 10 and 20 particles per square meter is sufficient.

The benefit of incorporating the phase-derived pseudorange data is apparent when comparing the performance of the navigation filter using only the OWTT data and the results using pseudorange measurements. Figure 9 shows how the



FIG. 5. (Color online) REMUS 100 vehicle used for this experiment is shown as it is being deployed. The hydrophone is visible at the vehicle nose. The modem hardware and passband recorder is incorporated within the vehicle's dry payload section (inside the yellow hull section).

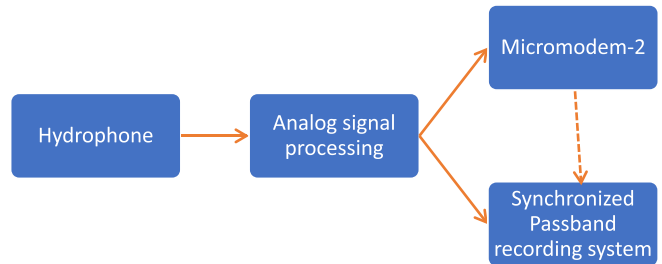


FIG. 6. (Color online) Block diagram of the recording system integrated in the REMUS AUV.

uncertainty of the position estimate (shown as the standard deviation of the estimate) decreases as a series of packets are received over a 25-min period. The use of phase-derived pseudorange measurements in addition to the OWTT causes the navigation estimate to converge much more quickly, using fewer received acoustic packets. It also performs well even when there are long intervals during which no packets are received. Therefore, this method is more suitable than operating with only OWTT measurements when acoustic packets are received only intermittently. Even when OWTT measurements are regularly available, using pseudorange data improves the certainty of the position estimate.

## C. Results without OWTT

The performance of the navigation system using only phase measurements within packets, and not OWTT measurements, was also evaluated. This represents situations

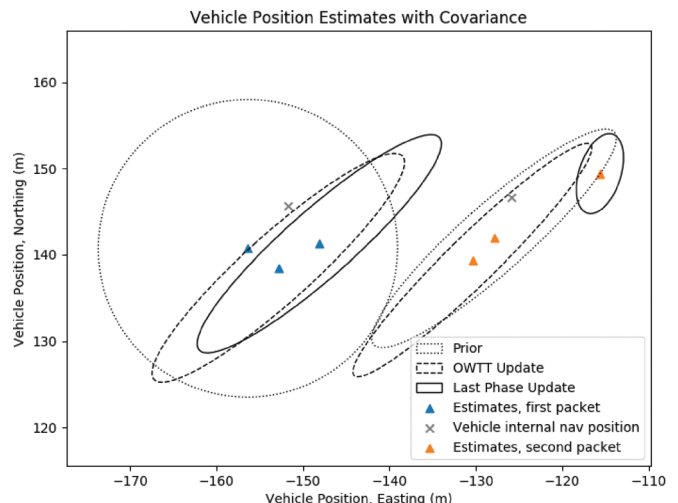


FIG. 7. Plot of estimates of vehicle position (triangles) and two-sigma covariance ellipses for the adaptive filter. As the vehicle travels east (left to right on the plot), two packets are received. Covariance ellipses are plotted showing the covariance of a prior estimate (the output of the predictor before measurements are incorporated) as a dotted line, a dashed ellipse showing the estimate once the OWTT measurement is incorporated, and a solid ellipse showing the estimate after all the phase measurements for the packet are incorporated. Many phase measurement updates are performed, but only the estimate after the last update is plotted for clarity. The decreasing area of the covariance ellipses shows how the filter incorporates data from OWTT measurements, as well as phase estimates, to improve the accuracy and confidence of the position estimate. The latest vehicle's internal navigation fix at the time of the last phase update is plotted for comparison. Inaccuracy in the survey of the LBL transponder and buoy positions during this experiment account for the differences among the position estimates.

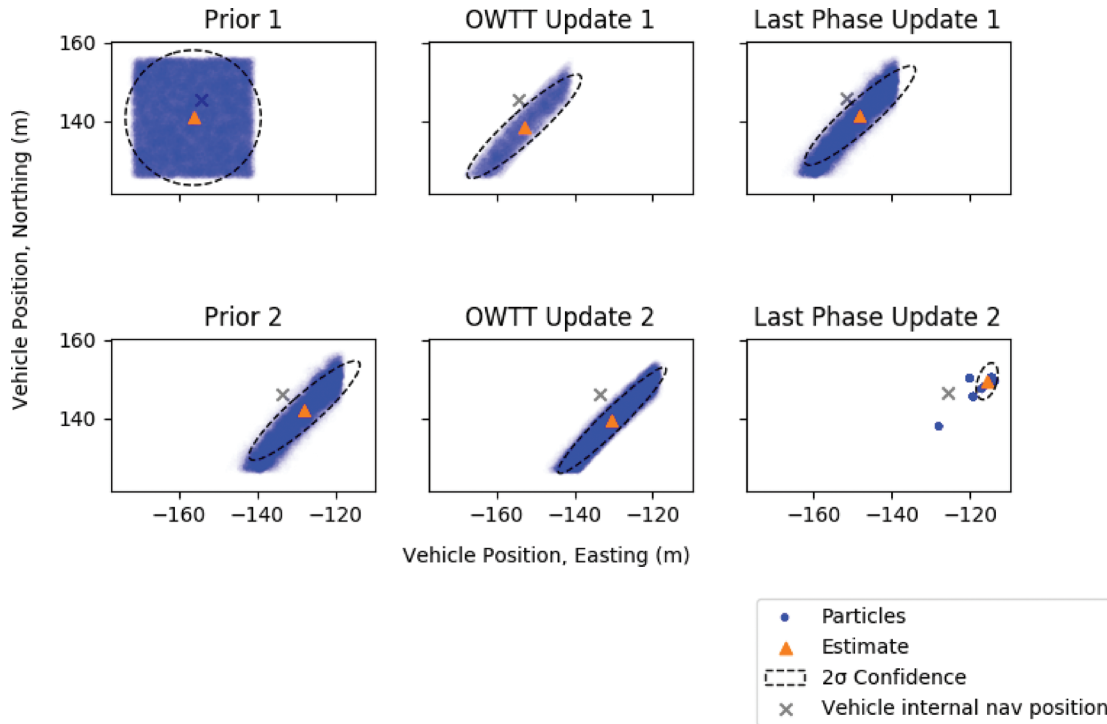


FIG. 8. Particle distributions with corresponding position estimates and covariance ellipses, shown as two packets, are received by the moving vehicle. This figure illustrates the same sequence as in Fig. 7, but it shows the particle cloud at each step. Each particle (blue dot) is partially transparent with its opacity determined by the weight of the particle. Therefore, more opaque regions correspond to higher-probability regions. The first subplot (“prior 1”) shows the user-provided initial particle distribution. The lower-right plot labeled, “last phase update 2,” shows that the additional phase measurements from the second packet allow the filter to converge.

where time is not accurately synchronized between the transmitter and receiver and, therefore, OWTT measurements are unavailable. Figure 10 shows a plot of localization estimates generated using only the phase-derived pseudorange data,

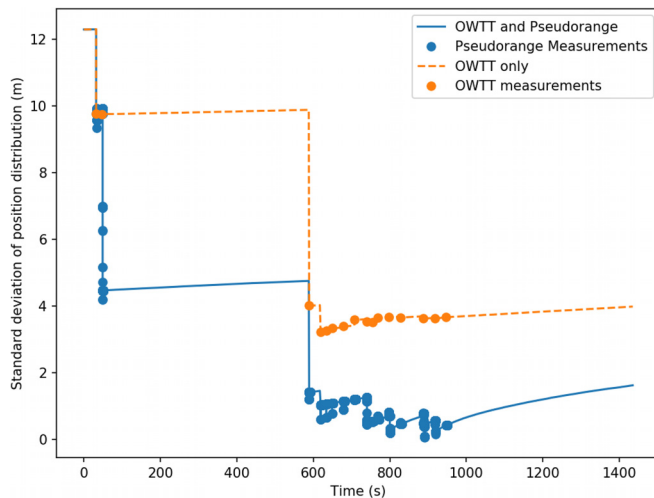


FIG. 9. (Color online) Weighted standard deviation [square root of the trace of Eq. (28)] of the position estimates generated by the filter. Results are shown for the cases where both pseudorange and OWTT measurements are used (blue solid line), and when only the OWTT measurements are used (orange dashed line). Phase measurement updates are highlighted using blue dot markers, and OWTT measurement updates are highlighted using orange dot markers. Note that uncertainty grows with time in the absence of new measurements, which can be seen in the areas where there are gaps between received packets (periods with no measurement markers). The reduction in uncertainty from using the phase measurements is apparent when comparing the results from the OWTT-only and OWTT-and-pseudorange measurement cases.

along with associated covariance ellipses and the vehicle’s internal navigation track.

When operating without OWTT, the filter still converges, but many additional measurements are needed to achieve levels of certainty in the position estimate comparable to the adaptive filter case described above, as shown in Fig. 11.

In both cases, the filter estimates converge to positions near the REMUS navigation algorithm estimates of position, which incorporated intermittent LBL navigation transponder fixes. The differences in position between the filter estimates and the REMUS algorithm are within the accuracy bounds of the experiment (several meters), which were limited by uncertainty in the position of LBL transponders and the transmitting buoy, all of which were manually surveyed using a handheld GPS. Future experimental validation could be performed on an instrumented tracking range to increase confidence in this algorithm.

## V. DISCUSSION

### A. Implementation details and limitations

The hybrid particle filter and UKF implementation used here is computationally advantageous, as it only tracks two state variables with particles, and it uses a single Kalman filter for tracking the motion of the vehicle. Field results from at-sea testing illustrate the performance of the approach and compatibility with the computational resources that can be available in most small AUVs. However, it does not model the non-zero covariance among the velocity, heading, and position states, and the Kalman-estimated state updates never incorporate pseudorange

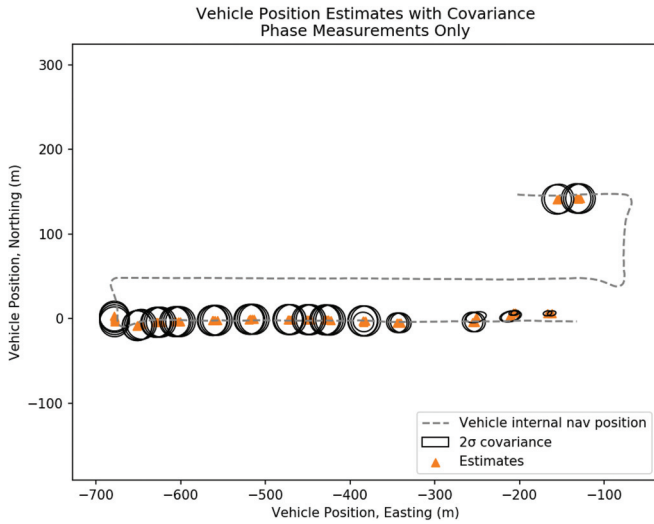


FIG. 10. Plot of estimates of vehicle position (triangles) and two-sigma covariance ellipses for the filter using only phase measurements. As the vehicle travels east and south (left to right, from top to bottom, on the plot), 16 packets are received, and the navigation filter runs continuously. Many phase measurement updates are performed, but only a few estimates per packet are plotted for clarity. The decreasing area of the covariance ellipses shows how the filter incorporates data from phase estimates to improve the confidence of the position estimate. The position estimate from the vehicle's internal navigation system is plotted as a gray dashed line. Note that measurements are only intermittently available (and entirely absent while the vehicle is traveling west), but the filter still tracks the vehicle position. The offset between the filter position estimate and the vehicle's internal navigation solution is about 12 m at the last estimate, which is within the accuracy bounds of this experiment.

data. Given greater computation capability in the future, better estimates might be found by converting the partitioned integrating filter into a marginalized (Rao-Blackwellized) particle filter or changing the partitioning such that more state variables are tracked by the particle filter.

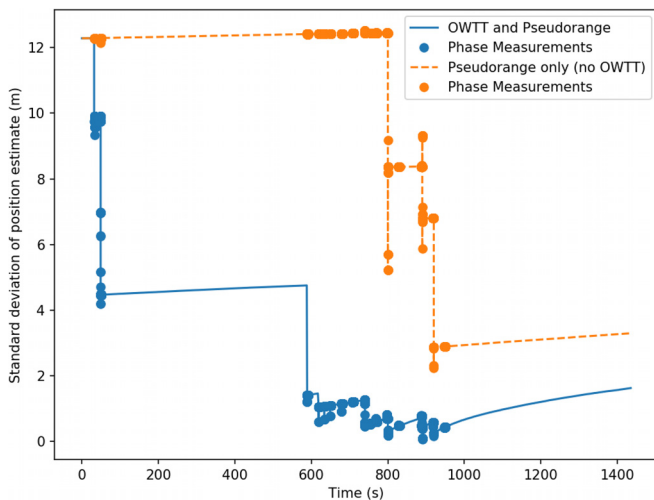


FIG. 11. (Color online) Weighted standard deviation [square root of the trace of Eq. (28)] of the position estimates generated by the filter, comparing the performance when OWTT is used (blue solid line) and when OWTT is not available (orange dashed line). Phase-derived pseudorange measurements are highlighted with dot markers (blue and orange). The certainty of the estimate improves as more data are incorporated by the filter in both cases, but the lack of OWTT data always increases the uncertainty of the estimate.

This choice of partition in state variables also allows the vehicle heading and velocity control inputs to the particle filter to be generated by another sensor fusion process in the vehicle, such as a separate inertial navigation system or the internal navigation algorithm. This is advantageous when only processed sensor data are readily accessible in the AUV and available sensor measurements may be delayed or decimated.

Although the phase tracking technique generates a new phase estimate for each symbol in the received packet, averaging and decimation is done to reduce the data output rate from the phase tracker. This process reduces the computational load by limiting the number of measurement updates performed by the particle filter. Furthermore, this system is designed for eventual real-time implementation, where the phase estimates will be provided by the Micromodem-2 to the computer running the navigation filter, and the communication throughput between these two devices is limited.

Additionally, measurements are gated for kinematic consistency and to avoid numerical effects associated with very small integration time steps.

Although this navigation method does not require that velocity over ground measurements from a DVL be continuously available, it does require a reasonable measurement or estimate of velocity over ground for the duration of a received packet. In the absence of these data, there is an inherent unresolvable ambiguity between the velocity over ground and the possible position tracks. Practically, this implies that the DVL must have continuous bottom lock, or the current must be sufficiently stationary that velocity through water measurements are sufficient to form accurate velocity over ground estimates at the time acoustic communication packets are received.

## B. Error in pseudorange measurement

Several significant sources contribute to error in the range measurement, including environmental uncertainty and timing accuracy. Timing errors in the phase measurement generate distance errors in the pseudorange measurement.

We use a single, measured value for the sound speed in the medium. This assumption is reasonable when operating over short ranges, but it would require propagation modeling to use the phase tracking technique in more challenging environments. A fractional error in sound speed corresponds to an error in range as

$$e_{\text{range}} = \frac{\bar{c}_{\text{used}} - \bar{c}_{\text{actual}}}{\bar{c}_{\text{actual}}} \rho, \quad (29)$$

where  $\rho$  is the actual range between the source and receiver, and  $\bar{c}$  is the average sound speed along the path.

Any mismatch in the sampling clock rate between the transmit and receive system will appear as a Doppler shift in the data. This offset propagates to range as

$$e_{\text{speed}} = c_s \frac{f_s^{\text{receiver}}}{f_s^{\text{source}}}, \quad (30)$$

$$e_{\text{range}} = e_{\text{speed}} t, \quad (31)$$

where  $t$  is at most the duration of the packet. In the system used for the experiment, the sample clock accuracy is at

worst  $\pm 20$  ppm, such that the maximum possible fractional difference between the source and receiver clock frequency is  $4E-5$ . Using typical values for sound speed, this error corresponds to a maximum Doppler velocity error of 6 cm/s and an accumulated range error of about 20 cm over the course of a packet. This error does not accumulate beyond the duration of a single packet.

The TOA estimate is affected primarily by the relative drift of the real-time clock in the system, which is accurate to  $\pm 2$  ppm on the Micromodem-2 (Gallimore *et al.*, 2010). This corresponds to the range error as

$$e_{\text{range}} = c \alpha_{\text{rtc}} t, \quad (32)$$

where  $\alpha_{\text{rtc}}$  is the drift rate of the real-time clock (bounded by the accuracy of the real-time clock), and  $t$  is the time since the real-time clock was last synchronized with a reference. Practically, the clock is synchronized to GPS time each time the vehicle surfaces. For example, for each hour that the vehicle has been submerged, the worst-case range error from this source is about 10 m.

Both the mismatch in sampling rate and real-time clock can be mitigated using a highly stable and accurate clock such as a CSAC (Gallimore *et al.*, 2012). The real-time clock drift can be mitigated using a more accurate real-time clock such as a SEASCAN (Eustice *et al.*, 2007).

Motion of either the vehicle or the transmitter that is not tracked by the model contributes directly to error in the navigation result. For example, if the transmit transducer is moving and that motion is not characterized, the changing range between the source and receiver appears as pseudorange error. Additionally, the kinematic model used may fail to accurately describe vehicle motion in highly dynamic conditions, where the kinematic assumptions might not hold. Once integrated, this will contribute to position error in the estimates.

### C. Possible extensions

In this paper, an algorithm for position estimation using phase measurements of acoustic communication signals is described, and experimental results are shown with a single transmitter at a fixed location and a moving receiver. This method is readily extended to the case of multiple transmitters and receivers. There is no limit imposed by the algorithm to the number of source-receiver pair phase measurements incorporated in the particle filter update. Although the transmitter was fixed and the moving platform hosted the receiver in this experiment, the algorithm operates symmetrically, and these roles could be reversed.

A less trivial extension would involve both a moving transmitter and receiver. While the fundamental approach remains the same, experimentation is required to determine how much kinematic information about the movement of the source must be transmitted to the receiver to generate useful position estimates.

## VI. CONCLUSIONS

A novel synthetic baseline navigation technique has been developed and demonstrated at sea. Analysis of

experimental results shows that the use of phase measurements from received acoustic communication packets will improve position estimates over those made using only a single OWTT measurement per packet. Furthermore, this technique can generate position estimates without using OWTT measurements, which are unavailable without synchronized transmitter and receiver clocks.

These benefits are realized using a modest amount of additional processing applied to existing signals measured by existing sensors. Therefore, this navigation technique is suitable for integration on production and experimental AUV platforms.

## ACKNOWLEDGMENTS

The authors wish to thank R. Hess, A. Nager, and N. Caruthers with the Scripps Institution of Oceanography for their efforts with vehicle integration and operation, and S. Singh, Dr. J. Partan, and R. Stokey at the Woods Hole Oceanographic Institution for their assistance with the acoustic modem system and REMUS vehicle. T. Schrameck and Dr. S. Merrifield at the Scripps Institution of Oceanography are thanked for providing feedback on this manuscript. This work was supported in part by the Office of Naval Research under Contract No. N00014-12-G-0136 and in part by the Friedkin Foundation. The work of E.G. was also supported in part by the Department of Defense (DoD) through the National Defense Science and Engineering Graduate Fellowship (NDSEG) Program.

<sup>1</sup>Corresponding to force, velocity, and pose of surge, sway, heave, roll, pitch, and yaw. Irrotational current requires another three velocity states; see, e.g., Gustafsson (2012).

- Austin, T. C. (1994). "The application of spread spectrum signaling techniques to underwater acoustic navigation," in *Proceedings of IEEE Symposium on Autonomous Underwater Vehicle Technology (AUV'94)*, pp. 443–449.
- Cappe, O., Godsill, S. J., and Moulines, E. (2007). "An overview of existing methods and recent advances in sequential Monte Carlo," *Proc. IEEE* **95**, 899–924.
- Eustice, R. M., Whitcomb, L. L., Singh, H., and Grund, M. (2006). "Recent advances in synchronous-clock one-way-travel-Time acoustic navigation," in *OCEANS 2006*, pp. 1–6.
- Eustice, R. M., Whitcomb, L. L., Singh, H., and Grund, M. (2007). "Experimental results in synchronous-clock one-way-travel-time acoustic navigation for autonomous underwater Vehicles," in *2007 IEEE International Conference on Robotics and Automation*, pp. 4257–4264.
- Fulton, T. (2000). "Acoustic navigation for the autonomous underwater vehicle REMUS," M.S. thesis, Massachusetts Institute of Technology, Cambridge, MA, available at <http://dspace.mit.edu/handle/1721.1/88342> (Last viewed 4/24/2016).
- Gallimore, E., Partan, J., Singh, S., Freitag, L., Ball, K., Koski, P., and Beal, A. (2012). "Developments in timing and satellite telemetry with the Micromodem-2," in *The 7th ACM International Conference on Underwater Networks and Systems (WUWNet '12)*, Los Angeles, CA.
- Gallimore, E., Partan, J., Vaughn, I., Singh, S., Shusta, J., and Freitag, L. (2010). "The WHOI micromodem-2: A scalable system for acoustic communications and networking," in *OCEANS 2010*, pp. 1–7.
- Gustafsson, F. (2010). "Particle filter theory and practice with positioning applications," *IEEE Aerosp. Electron. Syst. Mag.* **25**, 53–82.
- Gustafsson, F. (2012). *Statistical Sensor Fusion* (Studentlitteratur, Lund, Sweden), 543 pp.
- Hartsfield, J. C. (2005). "Single transponder range only navigation geometry (STRONG) applied to REMUS autonomous under water vehicles," M.S. thesis, Massachusetts Institute of Technology, Cambridge, MA, available at <http://calhoun.nps.edu/handle/10945/11055> (Last viewed 11/9/2019).

- Hol, J. D., Schon, T. B., and Gustafsson, F. (2006). "On resampling algorithms for particle filters," *2006 IEEE Workshop on Nonlinear Statistical Signal Processing*, pp. 79–82.
- Johnson, M., Freitag, L., and Stojanovic, M. (1997). "Improved Doppler tracking and correction for underwater acoustic communications," in *1997 IEEE International Conference on Acoustics, Speech, and Signal Processing, ICASSP-97*, Vol. 1, pp. 575–578.
- Julier, S. J., and Uhlmann, J. K. (1997). "New extension of the Kalman filter to nonlinear systems," *Proc. SPIE* **3068**, 182–193.
- Julier, S. J., and Uhlmann, J. K. (2004). "Unscented filtering and nonlinear estimation," *Proc. IEEE* **92**, 401–422.
- Larsen, M. B. (2000). "Synthetic long baseline navigation of underwater vehicles," in *OCEANS 2000 MTS/IEEE Conference and Exhibition*, Vol. 3, pp. 2043–2050.
- Quigley, M., Conley, K., Gerkey, B., Faust, J., Foote, T., Leibs, J., Wheeler, R., and Ng, A. (2009). "ROS: An open-source robot operating system," in *ICRA Workshop on Open Source Software*, Kobe, Japan, Vol. 3, No. 3.2, p. 5.
- Rigby, P., Pizarro, O., and Williams, S. B. (2006). "Towards geo-referenced AUV navigation through fusion of USBL and DVL measurements," in *OCEANS 2006*, pp. 1–6.
- Ristic, B., Arulampalam, S., and Gordon, N. (2004). *Beyond the Kalman Filter: Particle Filters for Tracking Applications* (Artech Print on Demand, Boston, MA), 318 pp.
- Simon, D. (2006). *Optimal State Estimation: Kalman, H Infinity, and Nonlinear Approaches* (Wiley-Interscience, Hoboken, NJ), 526 pp.
- Singh, S., Grund, M., Bingham, B., Eustice, R., Singh, H., and Freitag, L. (2006). "Underwater acoustic navigation with the WHOI Micro-Modem," in *OCEANS 2006*, pp. 1–4.
- Stojanovic, M., Catipovic, J. A., and Proakis, J. G. (1994). "Phase-coherent digital communications for underwater acoustic channels," *IEEE J. Ocean. Eng.* **19**, 100–111.
- Stojanovic, M., Freitag, L., Leonard, J., and Newman, P. (2002). "A network protocol for multiple AUV localization," in *OCEANS '02 MTS/IEEE*, Vol. 1, pp. 604–611.
- Teledyne RD Instruments (2016). "Workhorse Navigator Doppler Velocity Log (DVL) Datasheet," available at [http://rdinstruments.com/\\_documents/navigator\\_datasheet\\_hr\\_GL.pdf](http://rdinstruments.com/_documents/navigator_datasheet_hr_GL.pdf) (Last viewed 11/8/2016).
- Wan, E. A., and Merwe, R. V. D. (2000). "The unscented Kalman filter for nonlinear estimation," in *The IEEE Adaptive Systems for Signal Processing, Communications, and Control Symposium 2000, AS-SPCC*, pp. 153–158.
- Watanabe, Y., Ochi, H., and Shimura, T. (2012). "A study of inverse SSBL acoustic positioning with data transmission for multiple AUV navigation," in *OCEANS 2012—Yeosu*, pp. 1–6.
- Watanabe, Y., Ochi, H., Shimura, T., and Hattori, T. (2009a). "A tracking of AUV with integration of SSBL acoustic positioning and transmitted INS data," in *OCEANS 2009—EUROPE*, pp. 1–6.
- Watanabe, Y., Ochi, H., Shimura, T., and Hattori, T. (2009b). "Super short baseline underwater acoustic positioning supported by inertial navigation data using spread spectrum communication for autonomous underwater vehicle and error analysis in deep water," *Jpn. J. Appl. Phys.* **48**, 07GL01.
- Yang, T. C. (2015). "Source depth estimation based on synthetic aperture beamforming for a moving source," *J. Acoust. Soc. Am.* **138**, 1678–1686.